Active noise control of enclosed centrifugal blowers

J. James Esplin[a)], Scott D. Sommerfeldt[b)], Kent L. Gee[c)] and John K. Boyle[d)]

Global active noise control has been obtained on the tonal noise from a small centrifugal blower, similar to those used in laptop computers. Compact control systems were investigated for two configurations. The blower was mounted in both a short rectangular duct and in a mock laptop case that was modeled as a two-dimensional rectangular enclosure. Secondary sources and error sensors were located adjacent to the duct or inside the enclosure. Error sensor locations were guided by analytical models for minimization of power radiation from ducted or enclosed simple sources. This paper demonstrates the experimental verification of both of these models, which shows significant global sound power reduction of the blower's primary tone in both cases. © *2016 Institute of Noise Control Engineering.*

1 INTRODUCTION

Noise from information technology (IT) equipment is a significant problem in today's contemporary society[1]. From computers and projectors to printers and copiers, IT equipment noise permeates many facets of our everyday lives in a technology-driven world. Due to its prevalence, there is an intense interest in reducing, controlling and eliminating IT equipment noise in its many forms, including noise produced by fans of IT equipment[2]. IT fan noise can be reduced with a technique called active noise control (ANC).

ANC uses one or more controlled sources (called secondary sources) to reduce the radiation from an uncontrolled noise source (called a primary source). It does this by minimizing the total pressure at one or more discrete location(s). These locations are defined by the placement of ANC error sensors. One important design characteristic of a practical ANC system is the placement of near-field error sensors at locations which minimize the overall radiated sound power.

A promising technique for ANC error sensor placement was introduced by Gee and Sommerfeldt and applied to small axial fans[3,4]. This technique employed an analytical minimization of sound power for collections of simple sources; these sources were used to model acoustic radiation from loudspeakers surrounding a baffled fan. This analytical minimization resulted in optimal secondary source strengths. These were used to calculate the resulting pressure field in the near-field of the fan and secondary sources. When the minimized power condition was met, the pressure field showed in the near-field of the fan one or more pressure minima. These minima are the predicted optimal location(s) for near-field error sensor(s)[3,4]. Experimental verification of the technique resulted in both the recreation of the predicted near-field pressure and a significant reduction of the global radiated sound power[5].

Previous research applying ANC to centrifugal blowers has concentrated on large centrifugal blowers, such as those used in HVAC systems[6–9]. However, little research has applied ANC to small centrifugal blowers, such as those used in laptops[10] and none has used the error sensor placement technique developed by Gee and Sommerfeldt[3,4].

This paper applies the ANC error sensor placement strategy pioneered by Gee and Sommerfeldt to an enclosed small centrifugal blower. Two separate applications are presented and separate models are developed for each. Note that though both models employ the error sensor placement strategy introduced by Gee and Sommerfeldt[3,4], they each have different theoretical foundations, both from the models used by Gee and Sommerfeldt and from each other. The first application places a small duct on the blower exhaust. Its corresponding model was developed to control tonal noise radiated from the blower's exhaust. The second application places the blower inside of a mock laptop enclosure,

a) Department of Physics and Astronomy, N283 ESC, Brigham Young University, Provo, UT 84602, USA; email: james@jamesesplin.info.

b) Department of Physics and Astronomy, N283 ESC, Brigham Young University, Provo, UT 84602, USA; email: scott_sommerfeldt@byu.edu.

c) Department of Physics and Astronomy, N283 ESC, Brigham Young University, Provo, UT 84602, USA; email: kentgee@physics.byu.edu.

d) Department of Physics and Astronomy, N283 ESC, Brigham Young University, Provo, UT 84602, USA; email: jkb321@gmail.com.

which is treated as a two-dimensional rectangular enclosure. Its corresponding model was developed to control tonal noise from the blower's inlets as it radiates from the laptop's interior. Experimental verification of both models is presented. Both models showed significant reductions in radiated sound power when ANC error sensors were placed according to their recommendations.

2 THEORY

2.1 ANC of a Finite-Length Rectangular Duct

This section introduces a model which guides the placement of error sensors for ANC of a point source in a finite-length baffled rectangular duct. This model first solves for the radiated pressure due to a point source in the duct using the results given in Refs. 11–13. Then, the sound power radiated from the end of the duct is estimated. Next, the secondary source strength is optimized to minimize the radiated sound power. Finally, the ideal error sensor locations are identified based on the near-field pressure generated when the radiated sound power is minimized.

2.1.1 Geometry

The model geometry is shown schematically in Fig. 1. First, the centrifugal blower and the ANC loudspeaker are assumed to be point sources in a duct mounted in a baffle. This assumption is valid as long as both the blower's cutwater (the location where inlet flow is separated from outlet flow and the dominant tonal noise generator) and the ANC loudspeaker are much smaller than the wavelength of interest. The point sources are placed in a duct of dimensions $L_x \times L_y \times L_z$ with rigid boundaries in the x and y dimensions. The primary source (representing the blower) has a complex source strength Q_0 and is located at the point (x_0, y_0, z_0); the secondary source (the control loudspeaker) has a complex source strength Q_1 and is located at the point (x_1, y_1, z_1). The duct has a rigid boundary condition at $z = 0$ and a finite, non-zero radiation impedance boundary condition at $z = L_z$.

2.1.2 Determination of the radiated sound pressure

The first step is to determine the sound pressure in a duct due to a point source. This is done using the formulation derived in Refs. 11–13 and is given in:
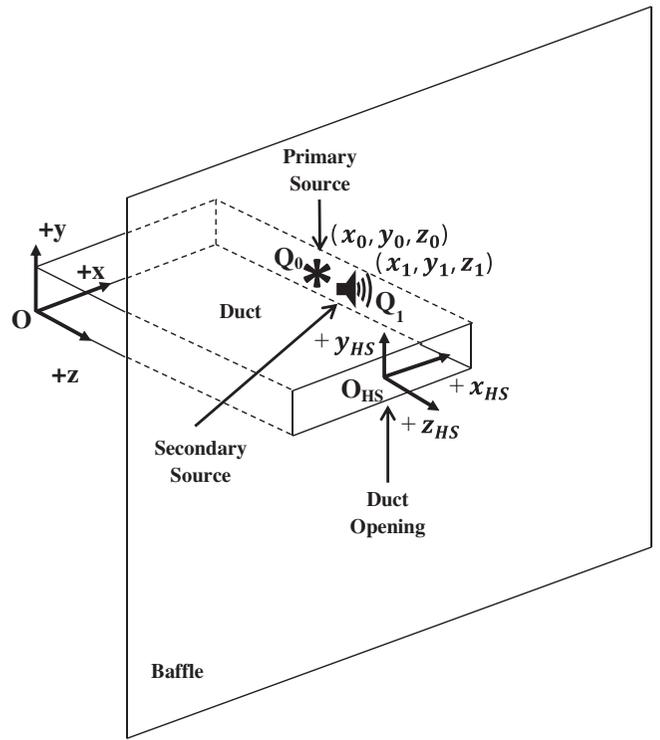

Fig. 1—Isometric view of the ideal system pictured with a primary source (modeling the blower) placed at (x_0, y_0, z_0) and secondary source (modeling the loudspeaker) located at (x_1, y_1, z_1) inside a rectangular duct mounted in an infinite baffle. The coordinate system inside the duct has its origin in the back left corner (at the point labeled O) and the coordinate system outside the duct (in the half-space) has its origin at the center of the duct's cross-section (at the point labeled O_{HS}).

where p is the complex pressure in the duct, ρ_0 is the ambient density, c is the ambient sound speed, k is the wavenumber and Q_0 is the complex source strength of the point source located at (x_0, y_0, z_0). m_x and m_y are modal indices in the x and y directions respectively and $\widetilde{k}_{z,m} = \sqrt{\widetilde{k}^2 - k_{m_x,m_y}^2}$, where $\widetilde{k}$ is the complex wavenumber and k_{m_x,m_y} is the wavenumber associated with the (m_x, m_y) mode. The variables $\widetilde{A}_m$ and $\widetilde{B}_m$ are complex modal weighting coefficients, given in Eqns. (2) and (3):

$$p(x,y,z|x_0,y_0,z_0) = j\rho_0 ckQ_0 \times \sum_{m_x,m_y=0}^{\infty} \cos\left(\frac{m_x\pi}{L_x}x\right)\cos\left(\frac{m_y\pi}{L_y}y\right)\left(\widetilde{A}_m e^{-j\widetilde{k}_{z,m}(z-z_0)} + \widetilde{B}_m e^{j\widetilde{k}_{z,m}(z-z_0)}\right), \qquad (1)$$

$$\widetilde{A}_m\left(\rho_0 ck - \widetilde{k}_{z,m}Z_{m,m}\right)e^{-j\widetilde{k}_{z,m}(L_z-z_0)}$$
$$+ \widetilde{B}_m\left(\rho_0 ck + \widetilde{k}_{z,m}Z_{m,m}\right)e^{j\widetilde{k}_{z,m}(L_z-z_0)}$$
$$= \sum_{n=0,n\neq m}^{\infty} \widetilde{k}_{z,n}Z_{m,n}\left(\widetilde{A}_n e^{-j\widetilde{k}_{z,n}(L_z-z_0)} - \widetilde{B}_n e^{j\widetilde{k}_{z,n}(L_z-z_0)}\right), \quad (2)$$

$$\left(\widetilde{k}_{z,m}\left[-j + \tan\left(\widetilde{k}_{z,m}z_0\right)e^{j\widetilde{k}_{z,m}(2z_0-L_z)}\right]\right)\widetilde{A}_m$$
$$+ \left(\widetilde{k}_{z,m}\left[j + \tan\left(\widetilde{k}_{z,m}z_0\right)e^{j\widetilde{k}_{z,m}(2z_0-L_z)}\right]\right)\widetilde{B}_m$$
$$= -\cos(m_x\pi\, x_0/L_x)\cos(m_y\pi\, y_0/L_y)/L_xL_y\Lambda_m, \quad (3)$$

where $Z_{m,n}$ is the radiation impedance at the duct's outlet at the $m = (m_x, m_y)$ pressure cross-sectional mode and $n = (n_x, n_y)$ particle velocity cross-sectional mode[14] and

$$\Lambda_m = \begin{cases} 1, & m_x = 0 \text{ and } m_y = 0 \\ 1/2, & m_x \neq 0 \text{ or } m_y \neq 0 \\ 1/4, & \text{otherwise} \end{cases} \quad (4)$$

The sum in Eqn. (2) includes both pressure cross-sectional modes (the m indices) and particle velocity cross-sectional modes (the n indices). The radiation impedance boundary condition at $z = L_z$ causes modal coupling between pressure modes and particle velocity modes. For a full derivation, see Refs. 11–13.

2.1.3 Minimization of radiated sound power

Minimizing the sound power radiated from the duct is the next step. This requires the addition of a secondary source, located at $r_1 = (x_1, y_1, z_1)$ with a complex source strength Q_1. This means that the total pressure inside the duct p_{tot} is given by:

$$p_{tot} = j\rho_0 ck[Q_0 G(r|r_0) + Q_1 G(r|r_1)]. \quad (5)$$

In Eqn. (5) $r = (x, y, z)$ is the field point, $r_0 = (x_0, y_0, z_0)$ is the location of the primary source and $G(r|r_0)$ is the Green's function between the source point r_0 and the field point r. The Green's function $G(r|r_0)$ is the split summation in Eqn. (1), given in Eqn. (6):

$$G(x, y, z|x_0, y_0, z_0) = \sum_{m_x, m_y=0}^{\infty} \cos\left(\frac{m_x\pi}{L_x}x\right)\cos\left(\frac{m_y\pi}{L_y}y\right)\left(\widetilde{A}_m e^{-j\widetilde{k}_{z,m}(z-z_0)} + \widetilde{B}_m e^{j\widetilde{k}_{z,m}(z-z_0)}\right). \quad (6)$$

The total sound power Π radiated from the duct is equal to:

$$\Pi = \int_0^{L_x}\int_0^{L_y} \frac{1}{2}\mathfrak{R}\left\{p_{tot}(x,y,L_z)u_z^*(x,y,L_z)\right\} dy\, dx, \quad (7)$$

where u_z is the total particle velocity in the z direction, r is expanded into its Cartesian components, $\mathfrak{R}$ denotes the real part, * denotes the complex conjugate and both p and u_z are evaluated at $z = L_z$.

From Eqn. (5) the particle velocity in the z direction is found through Euler's relation, given by:

$$u_z = -\left[Q_0\frac{\partial G(r|r_0)}{\partial z} + Q_1\frac{\partial G(r|r_1)}{\partial z}\right]. \quad (8)$$

Equations (5) and (8) are substituted into Eqn. (7), which leads to Eqn. (9):

$$\Pi = \frac{\rho_0 ck}{2}\int_0^{L_x}\int_0^{L_y}\mathfrak{I}\left\{|Q_0|^2 G(r|r_0)\frac{\partial G^*(r|r_0)}{\partial z} + \left(Q_0 G(r|r_0)\frac{\partial G^*(r|r_1)}{\partial z}\right)Q_1^* \right.$$
$$\left. + \left(G(r|r_1)Q_0^*\frac{\partial G^*(r|r_0)}{\partial z}\right)Q_1 + \left(G(r|r_1)\frac{\partial G^*(r|r_1)}{\partial z}\right)|Q_1|^2 \right\} dy\, dx, \quad (9)$$

where $\mathfrak{I}\{\ \}$ denotes the imaginary part of the quantity inside the brackets.

Equation (9) is an expression for the total radiated sound power Π in terms of the secondary source strength Q_1. To optimize Q_1 to minimize the radiated sound power it is first separated into its real and imaginary parts. This leads to:

$$\Pi = \rho_0 ck\,\mathfrak{I}\left\{A + BQ_{1,R} - jBQ_{1,I} + CQ_{1,R} \right.$$
$$\left. + jCQ_{1,I} + D|Q_1|^2\right\}/2, \quad (10)$$

where A, B, C and D are the quantities that multiply powers of Q_1 as shown in Eqn. (9). Note that the double integral is incorporated into each term of the sum.

The derivative of Π in Eqn. (10) is then taken with respect to both $Q_{1,R}$ and $Q_{1,I}$, which leads to:

$$\partial\Pi/\partial Q_{1,R} = \rho_0 ck\,\mathfrak{I}\left\{B + C + 2DQ_{1,R}\right\}/2 \text{ and } (11)$$

$$\partial\Pi/\partial Q_{1,I} = \rho_0 ck\,\mathfrak{I}\left\{-jB + jC + 2DQ_{1,I}\right\}/2. \quad (12)$$

Equations (11) and (12) are set equal to zero to optimize $Q_{1,R}$ and $Q_{1,I}$. This leads to:

$$Q_{1,R} = -(\Im\{B\} + \Im\{C\})/2\Im\{D\} \quad \text{and} \quad (13)$$

$$Q_{1,I} = (\Re\{B\} - \Re\{C\})/2\Im\{D\}. \quad (14)$$

The optimum complex secondary source strength is given by $Q_1 = Q_{1,R} + jQ_{1,I}$, which leads to:

$$
\begin{aligned}
Q_1 &= j\frac{B - C^*}{2\Im\{D\}}\\
&= j\frac{Q_0}{2}\frac{G(r|r_0)\partial G^*(r|r_1)/\partial z - G^*(r|r_1)\partial G(r|r_0)/\partial z}{\Im\{G(r|r_1)\partial G^*(r|r_1)/\partial z\}},
\end{aligned}
$$
$$(15)$$

where the Green's function $G(r|r_i)$ is as given in Eqn. (6). This is the secondary source strength that will minimize the sound power radiated from the finite-length duct.

2.1.4   Determination of error sensor locations

The final step is to determine the ideal location(s) for ANC error sensors. These locations are given by the nodal lines formed by the pressure field outside the duct when the radiated sound power is minimized. This pressure field is determined with Rayleigh's integral, given by:

$$p_{HS}(r_{HS}) = \frac{j\rho_0 ck}{2\pi}\int_0^{L_x}\int_0^{L_y} u_z(x,y,L_z)\frac{e^{-jkR(x,y)}}{R(x,y)}\,dy\,dx, \quad (16)$$

where p_{HS} is the pressure radiated from the duct into the half-space, r_{HS} is the coordinate system in the half-space (as seen in Fig. 1) and R is the distance from the source point (x_{HS}, y_{HS}) to the field point r_{HS}.

Equation (15) is substituted into Eqn. (8) and evaluated at $z = L_z$, which leads to:

$$u_z(L_z) = -[Q_0\partial G(r|r_0)/\partial z + Q_1\partial G(r|r_1)/\partial z]|_{z=L_z}. \quad (17)$$

Equation (17) is substituted into Eqn. (16), which leads to the pressure field outside the duct when the minimum radiated power condition is satisfied. This pressure field will contain nodal lines which denote the optimum locations for ANC error sensors.

When this analysis is applied, a figure such as Fig. 2 is the result. Figure 2 shows the decibel ratio of the near-field pressure along the surface of the baffle when the radiated sound power is minimized and divided by the original near-field pressure. The nodal line shows the optimal locations to place error sensors, as this line is generated when the radiated sound power is minimized. Note that these nodal lines are not present in
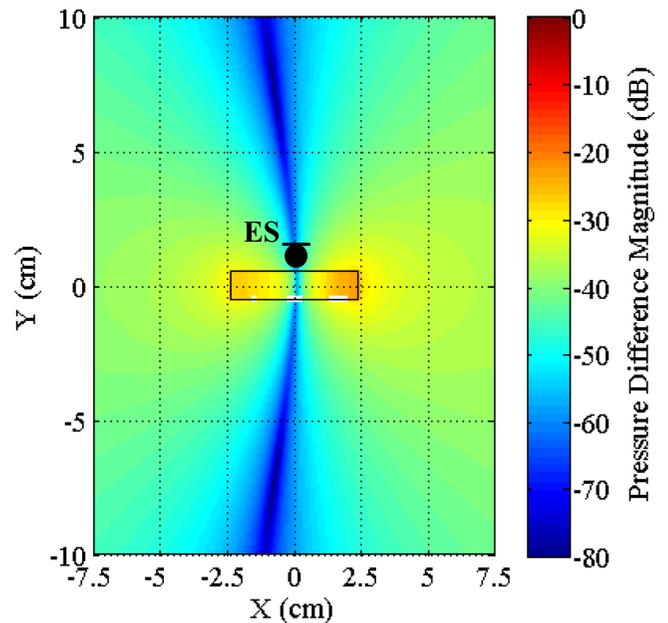

Fig. 2—Map of the decibel ratio of the pressure at 1 kHz when the radiation from the finite-length duct is minimized to the uncontrolled pressure. The rectangle in the middle represents the opening of the duct. For experimental validation, an error sensor (ES) is placed along the nodal line as indicated. Axis units are in centimeters while the color scale is in dB relative to the uncontrolled field.

the uncontrolled field and appear only when the minimum radiated sound power condition is met. This particular analysis was done at a frequency of 1 kHz, which is the blade passage frequency (bpf) of the centrifugal blower under test. Error sensor locations for other frequencies can be determined by evaluating the model output at those frequencies, plotting the same decibel ratio as described above and identifying the locations of nodal lines generated when the minimum radiated sound power condition is met.

2.2   ANC of a Two-Dimensional (2-D) Rectangular Enclosure

This section introduces a model which guides the placement of error sensors for ANC of a point source in a 2-D rectangular enclosure with lossy boundaries. This model first determines the radiated pressure due to a single point source in the enclosure. Next, the sound power radiated from the enclosure is estimated and minimized. Finally, ideal ANC error sensor locations are identified based on the near-field pressure generated when the radiated power is minimized.

2.2.1 Geometry

The model geometry is shown schematically in Fig. 3. Both the centrifugal blower and the ANC loudspeaker are modeled as point sources inside a mock laptop enclosure of dimensions $\mathcal{L}_x \times \mathcal{L}_y \times \mathcal{L}_z$. Because the wavelengths of the frequencies of interest are much larger than the smallest dimension of this enclosure (assumed

$$p(x,y) = -j\rho_0 ckQ \sum_{\mathbb{L}=0}^{\infty} \frac{\cos(l_x \pi \, x_0/\mathcal{L}_x)\cos(l_y \pi \, y_0/\mathcal{L}_y)}{\left(k^2 - \widetilde{k}_{\mathbb{L}}^2\right)\mathcal{L}_x \mathcal{L}_y \Lambda_{\mathbb{L}}} \cos\left(\frac{l_x \pi}{\mathcal{L}_x}x\right)\cos\left(\frac{l_y \pi}{\mathcal{L}_y}y\right), \tag{18}$$

to be $\mathcal{L}_z$), it is neglected in the analysis. This leaves a collection of point sources inside a two-dimensional rectangular enclosure with dimensions $\mathcal{L}_x \times \mathcal{L}_y$. Sound radiates from ports on the mock laptop enclosure which are located along the boundaries at $x = 0$ and $x = \mathcal{L}_x$. The radiation from these ports can be modeled by incorporating damping into the model along these boundaries. Thus boundaries at $x = 0$ and $x = \mathcal{L}_x$ are assumed to be

lossy, while the boundaries at $y = 0$ and $y = \mathcal{L}_y$ are assumed to be rigid.

2.2.2 Determination of radiated pressure

The pressure radiated from a point source in a 2-D rectangular enclosure with lossy boundaries as derived in Ref. 15 are given in Eqn. (18):

where p is the pressure, ρ_0 is the density, c is the sound speed, k is the wavenumber, Q is the complex source strength of the point source and the modal index $\mathbb{L}$ is composed of the ordered pair (l_x, l_y). $\Lambda_{\mathbb{L}}$ is the spatial average of the cross-sectional eigenfunctions over the area $\mathcal{L}_x \mathcal{L}_y$, given by:

$$\Lambda_{\mathbb{L}} = \begin{cases} 1, & l_x = 0 \text{ and } l_y = 0 \\ 1/2, & l_x \neq 0 \text{ or } l_y \neq 0 \\ 1/4, & \text{otherwise} \end{cases} . \tag{19}$$

The complex modal wavenumber $\widetilde{k}_{\mathbb{L}}$ is given by:

$$\widetilde{k}_{\mathbb{L}}^2 = (l_x \pi/\mathcal{L}_x + j\,\delta_b/c)^2 + \left(l_x \pi/\mathcal{L}_y\right)^2, \tag{20}$$

where δ_b is a constant proportional to the radiation damping of the boundaries in x. If the boundaries in y were also lossy, there would be another imaginary term inside the second set of parentheses in Eqn. (20). For a full derivation, see Ref. 15.

2.2.3 Minimization of radiated sound power & determination of error sensor locations

Next, the power radiated from the enclosure must be determined and minimized. The radiated power is equivalent to the power dissipated by the losses in the model. Using the source coupling concept developed by Nelson and Elliott[16], the total power radiated from the enclosure is given by:

$$\Pi = Q^H \Re\{Z^H\}Q/2, \tag{21}$$

where Q is the vector of complex source strengths, ^{H} denotes the Hermitian operator, $\Re\{\ \}$ denotes the real part and the elements of Z are given in Eqn. (22);
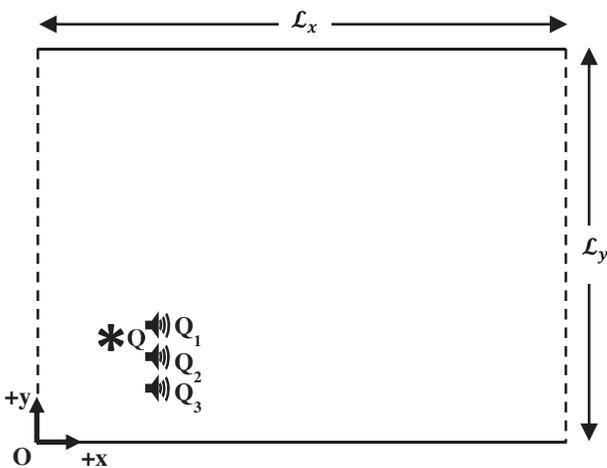

Fig. 3—Drawing of the two-dimensional rectangular enclosure the model simulates. The rectangular enclosure has dimensions $\mathcal{L}_x \times \mathcal{L}_y$ and lossy boundaries are located at $x = 0$ and $x = \mathcal{L}_x$. The primary source that models the blower is located as indicated with a source strength Q, while secondary sources are placed as shown with source strengths Q_1, Q_2 and Q_3.

$$Z_{i.j} = -j\rho_0 ck \sum_{\mathbb{L}=0}^{\infty} \frac{\cos(l_x \pi \, x_i/\mathcal{L}_x)\cos(l_y \pi \, y_i/\mathcal{L}_y)\cos(l_x \pi \, x_j/\mathcal{L}_x)\cos(l_y \pi \, y_j/\mathcal{L}_y)}{\left(k^2 - \widetilde{k}_{\mathbb{L}}^2\right)\mathcal{L}_x \mathcal{L}_y \Lambda_{\mathbb{L}}}. \tag{22}$$

Note that Eqn. (22) is merely the pressure generated at source i due to source j as given by Eqn. (18) divided by the source strength Q_i.

Equation (21) is separated into primary and secondary components, given by:

$$\Pi = \left[\boldsymbol{Q}_p^H \Re\left\{\boldsymbol{Z}_{p,p}^H\right\} \boldsymbol{Q}_p + \boldsymbol{Q}_p^H \Re\left\{\boldsymbol{Z}_{p,s}^H\right\} \boldsymbol{Q}_s + \boldsymbol{Q}_s^H \Re\left\{\boldsymbol{Z}_{s,p}^H\right\} \boldsymbol{Q}_p + \boldsymbol{Q}_s^H \Re\left\{\boldsymbol{Z}_{s,s}^H\right\} \boldsymbol{Q}_s \right]/2. \tag{23}$$

The terms in Eqn. (23) from left to right correspond to self-coupling between the primary sources, then mutual coupling from the primary to the secondary sources, mutual coupling from the secondary to the primary sources and self-coupling between the secondary sources.

Now the overall power Π must be minimized. To do this, the derivative of Eqn. (23) is taken with respect to $\boldsymbol{Q}_s$ and set equal to zero:

$$\partial\Pi/\partial\boldsymbol{Q}_s = \left[2\Re\left\{\boldsymbol{Z}_{s,p}^H\right\}\boldsymbol{Q}_p + 2\Re\left\{\boldsymbol{Z}_{s,s}^H\right\}\boldsymbol{Q}_{s_O}\right]/2 = \boldsymbol{0} \Rightarrow$$
$$\boldsymbol{Q}_{s_O} = \Re\left\{\boldsymbol{Z}_{s,s}^H\right\}^{-1} \Re\left\{\boldsymbol{Z}_{s,p}^H\right\}\boldsymbol{Q}_p, \tag{24}$$

where $\boldsymbol{Q}_{s_O}$ is the optimal secondary source strength needed to minimize the radiated sound power.

When Eqn. (24) is substituted into an expanded form of Eqn. (18), this leads to:

$$p(r) = -j\rho_0 ck \sum_{\mathbb{L}=0}^{\infty} \frac{\sum_p Q_p \Psi_{\mathbb{L}}(r_p) + \sum_s Q_{s_o} \Psi_{\mathbb{L}}(r_s)}{\left(k^2 - \widetilde{k}_{\mathbb{L}}^2\right)\mathcal{L}_x \mathcal{L}_y \Lambda_{\mathbb{L}}} \Psi_{\mathbb{L}}(r), \tag{25}$$

where r_p and r_s denote the locations of the primary and secondary sources respectively. The sums over p and s in the numerator of the fraction denote summing over all primary and secondary sources respectively.

Equation (25) describes the pressure field which is a consequence of the minimum power condition. Its result leads to Fig. 4, which shows the decibel ratio of the near-field pressure generated when the sound power is minimized to the original near-field pressure at a frequency of 1 kHz (the bpf of the centrifugal blower) for the source configuration pictured in Fig. 3. As before, these nodal lines are not present in the uncontrolled field and appear only when the minimum radiated sound power condition is met. The nodal lines shown are the ideal locations for placement of ANC error sensors, as these lines are generated when the sound power is minimized. As before, error sensor locations for other frequencies can be determined by evaluating the model output at those frequencies, plotting the same decibel

ratio as described above and identifying the locations of nodal lines generated when the minimum radiated sound power condition is met.

3 EXPERIMENT

The experimental validations of the models derived in Sec. 2 are presented in this section. First, elements common to both experiments are presented. These elements include the characteristics of the centrifugal blower, details on the ANC system, the rotating microphone array used to measure sound power and the metric used to validate the models (radiated sound power reduction). Next, the experiment used to validate the finite-length rectangular duct model is described. This model was developed to control the noise radiated from the blower's exhaust. Thus, the experiment was designed to measure only noise radiated from the blower's exhaust. Lastly, the experiment used to validate the two-dimensional rectangular enclosure is presented. This model was developed to control the noise radiated from the blower's
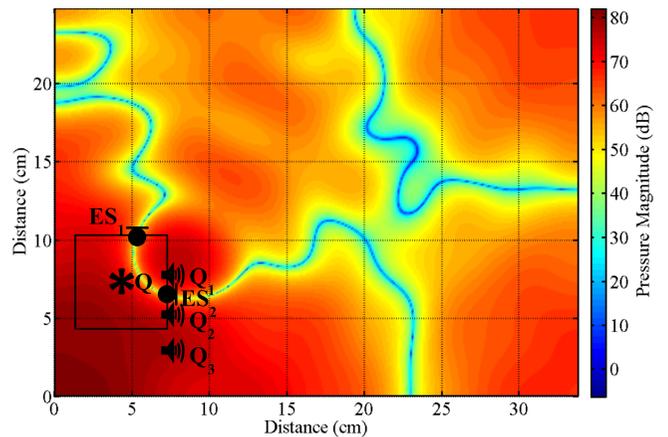

Fig. 4—Map of the decibel ratio of the pressure at 1 kHz when the radiation from the rectangular enclosure is minimized to the uncontrolled pressure. The square in the bottom-left represents the blower, while the secondary sources are placed in the locations indicated. For experimental validation, error sensors are placed along nodal lines as indicated. Axis units are in centimeters while the color scale is in dB relative to the uncontrolled field.

inlets. Thus, the experiment was designed to measure only the blower's inlet noise.

3.1 General Experimental Setup

The centrifugal blower used in this study (pictured in Fig. 5) is approximately 6 cm × 6 cm × 1 cm and has an outlet which is 4.8 cm wide and 1 cm high. It has a bpf of approximately 1 kHz when operating at its design voltage. Its cutwater is identified in Fig. 5. Its uncontrolled sound power output is shown in Fig. 6.

The ANC system used for these tests employs a filtered-x least-mean-squared algorithm along with offline system identification. Its sampling frequency is set at 6 kHz. Details of the algorithm are given in Ref. 17.

All experiments were performed in an anechoic chamber. This anechoic chamber is fitted with a rotating semi-circular arc. Thirteen 12.77 mm GRAS free-field, Type-1 microphones were attached to this arc at 15° increments. The microphones were attached to the arc on thin metal rods to minimize scattering and were placed 56 cm from the center of the arc.
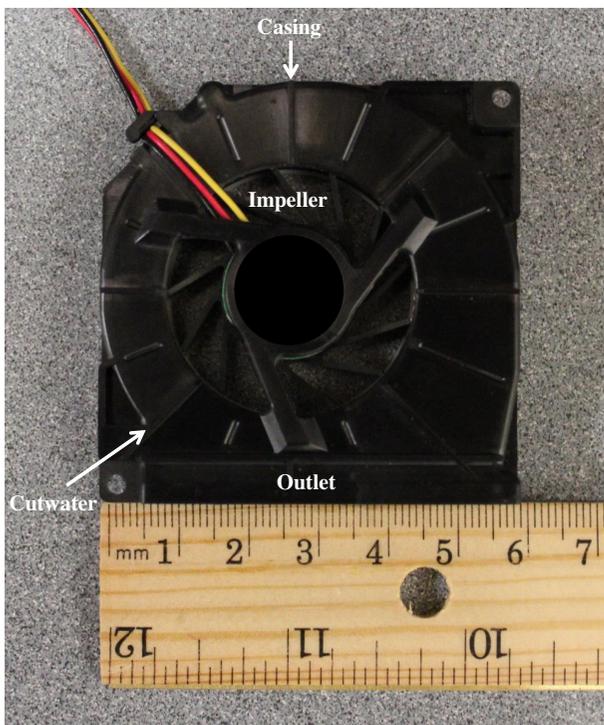

Fig. 6—*Typical noise spectrum for the centrifugal blower tested. The motor speed for this spectrum is approximately 75 Hz, while its blade passage frequency (bpf) is at approximately 1000 Hz. The horizontal axis is frequency in Hz and the vertical axis is sound power level in dB.*

Fig. 5—*Photograph of the centrifugal blower used in this study. Airflow is directed into the blower perpendicular to the page and is pushed by its impeller through its outlet. The blower's casing, impeller, cutwater and outlet are indicated. The ruler is included for scale.*
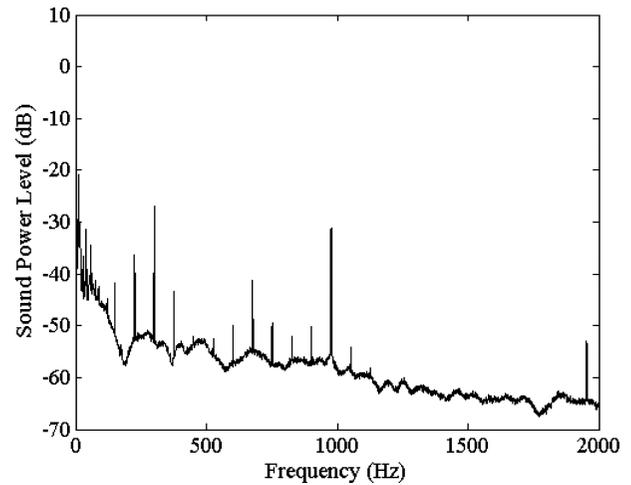
Both experiments were designed to measure the reduction in radiated sound power. The sound power is proportional to 10 times the common logarithm of the sum of the squared pressures measured over a hemisphere. The square pressures were weighted such that those near the bottom of the arc (which sweep out over more area) are weighted higher than those near the top of the arc (which sweep out over less area). This is known as equal-area weighting and is explained in Ref. 18. By taking the difference between this value without and with ANC, the overall sound power level reduction was obtained.

3.2 Experimental Validation of the Finite-Length Rectangular Duct Model

This model (described in Sec. 2.1) was verified experimentally in two different stages. The first stage was to apply the model to loudspeakers mounted in a wooden duct with the same approximate internal dimensions as the centrifugal blower and its attached duct. The second stage was to apply the model to the actual centrifugal blower and its attached duct.

The wooden duct (shown in Fig. 7) has internal dimensions of 4.8 cm × 1 cm × 10 cm. Two Sonion 0935 loudspeakers were inserted inside the duct in close proximity to each other—one for the primary source (placed 5.75 cm from the duct's rigid end) and one for the secondary source (placed 6.25 cm from the duct's rigid end on the same side as the primary source). This duct was mounted in a large baffle (2.29 m × 2.29 m)
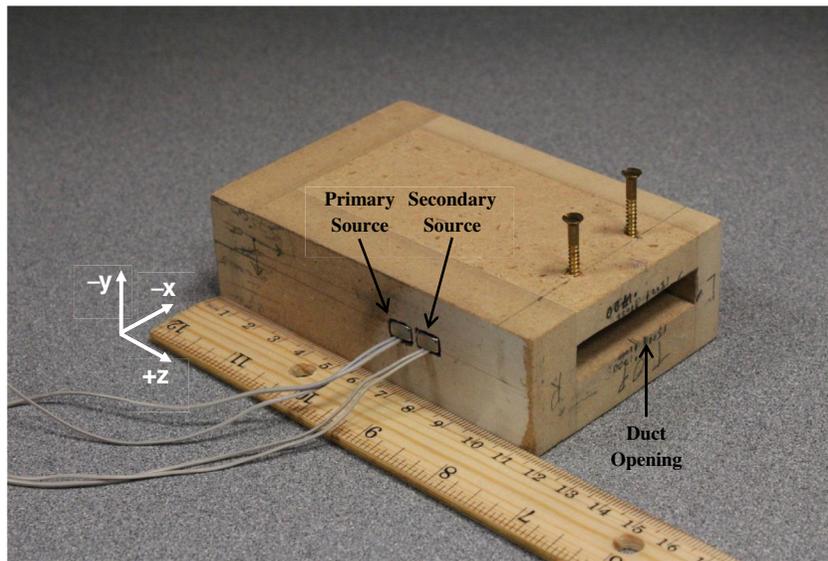
Fig. 7—Picture of the ideal duct used to validate the model. Note the primary source and secondary source on the left side of the duct. The ruler is included for scale.

underneath a rotating semicircular arc. The error sensor (3.15 mm diameter electret microphone) was placed on the baffle in the ideal location predicted by the model, shown in Fig. 2 (approximately 1 cm above the center of the duct outlet). The microphone array, baffle and duct are shown in Fig. 8. The sound power of the system was measured with the rotating microphone arc shown in Fig. 8 both with and without ANC. The difference in these two values is the overall sound power level reduction.

Recall that this model was developed to control the exhaust noise of the ducted centrifugal blower. The centrifugal blower and duct assembly is pictured in Fig. 9. This assembly was mounted in the same 2.29 m × 2.29 m baffle (pictured in Fig. 8) with the error sensor in the same location as before. The exhaust of the blower was vented above the baffle. A Sonion 0935 loudspeaker was used as the secondary source. The error sensor was placed in the same location as shown in Fig. 2 (approximately 1 cm above the center of the blower exhaust). As before, the sound power of the system was measured with the rotating microphone arc shown in Fig. 8 both with and without ANC. The difference in these two values is the overall sound power level reduction.
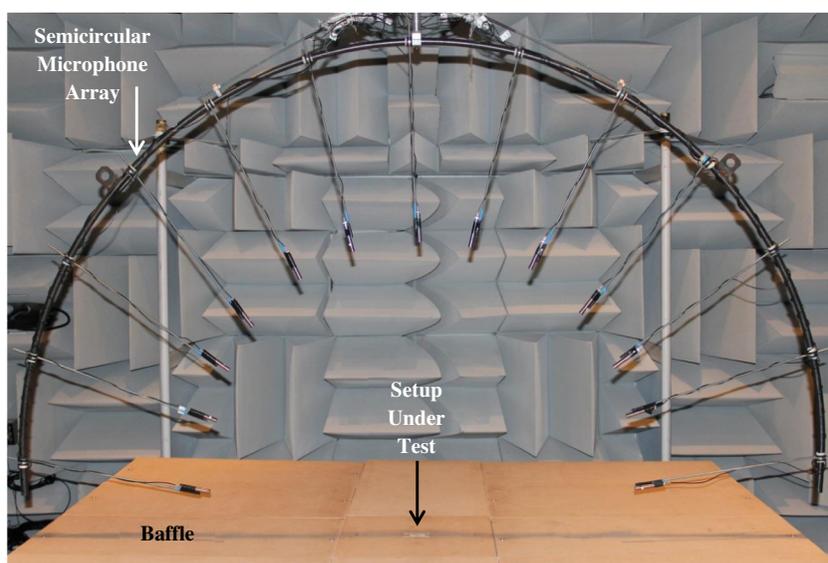

Fig. 8—Photograph showing the ideal duct mounted underneath a large baffle (2.29 m × 2.29 m) with a semicircular rotating array of microphones (56 cm radius) suspended overhead.
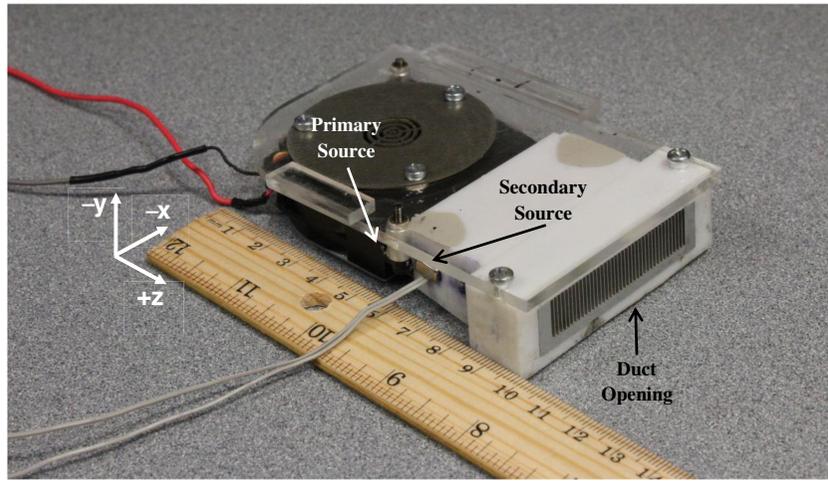
Fig. 9—Photograph of the blower and duct assembly used in the second stage of testing. Note the secondary source on its left side, located just downstream of the blower's cutwater. The ruler is included for scale.

3.3 Experimental Validation of the 2-D Rectangular Enclosure Model

To verify this model (described in Sec. 2.2) experimentally, the blower, secondary sources (Regal R-15-E, 2.54 cm diameter) and error sensors (3.15 mm diameter electret microphones) were placed in the mock laptop enclosure (pictured in Fig. 10). This enclosure has dimensions 33.82 cm × 24.77 cm × 2.54 cm. The primary source was assumed to be at the center of the fan's inlet, located at $(x, y) = (4.3, 7.3)$ cm. Secondary sources were placed at $(x, y) = (7.5, 7.3)$ cm, $(7.5, 5.3)$ cm and $(7.5, 3.3)$ cm. All distances are measured from the bottom-left corner of the enclosure as seen in Figs. 3 and 10. Two different configurations were used for the error sensors. The first configuration is shown in Fig. 4 and follows the model's recommendations, with error sensors at $(x, y) = (5.2, 10.2)$ cm and $(7.5, 6.3)$ cm. These locations were chosen because they lay on top of the nodal line seen in Fig. 4 while remaining in close proximity to the secondary sources. The second configuration is shown in Fig. 11 and does not follow the model's
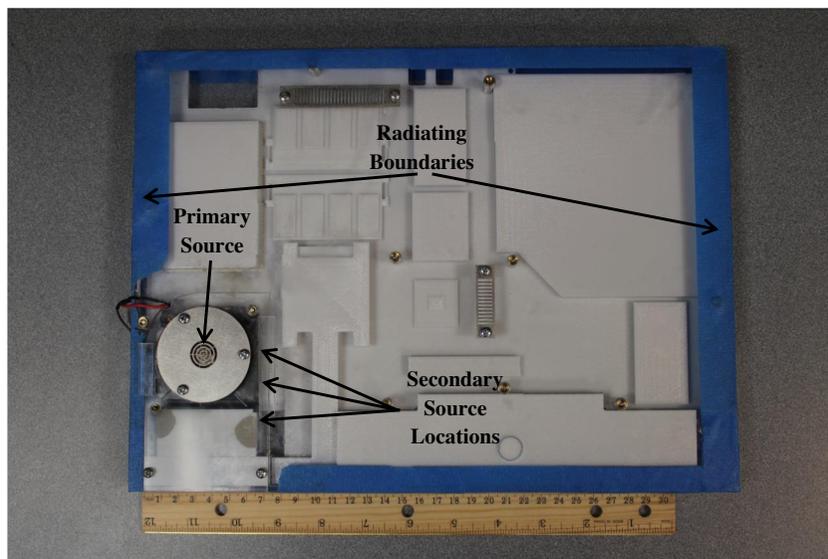

Fig. 10—Photograph of the mock laptop enclosure. The blower and duct assembly is mounted in the bottom-left corner of the enclosure. Noise is radiated from ports located on the left and right side of the mock laptop enclosure. The primary source (centrifugal blower) and secondary source locations are annotated, as are the boundaries that radiate sound (due to the presence of the aforementioned ports). The ruler is included for scale.
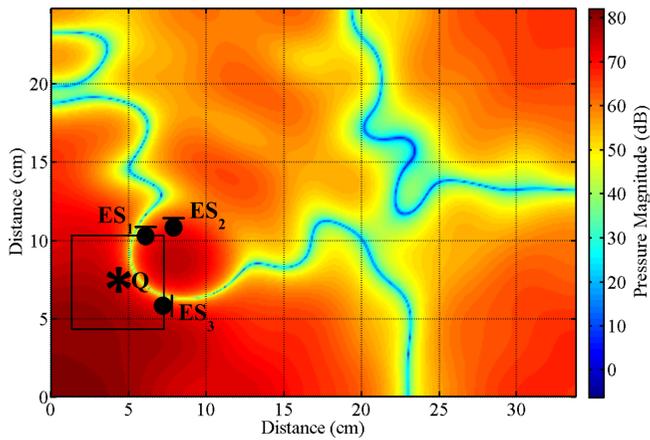
Fig. 11—*Incorrect error sensor positions used to validate the two-dimensional modal model. The decibel ratio of the pressure when the radiation from the rectangular enclosure is minimized to the uncontrolled pressure is shown for reference. The square in the bottom-left represents the blower. Axis units are in centimeters while the color scale is in dB.*

recommendations, with error sensors at approximately $(x, y) = (6.0, 10.2)$ cm, $(8.0, 11.0)$ cm and $(7.5, 5.8)$ cm. The second configuration uses the same primary and secondary source locations as the first configuration—only the error sensor locations change.

The experimental setup is shown in Fig. 12. The enclosure was mounted in the same large baffle and underneath the same rotating array described Sec. 3.2. Recall that this model was developed to control the noise radiated from the blower's inlets. Thus, the exhaust of the enclosed centrifugal blower was vented below the baffle. The sound power of the system was measured with the aforementioned microphone arc both with and without ANC. The overall sound power reduction was obtained by taking the difference in sound power both without and with ANC.

4 RESULTS

4.1 Finite-Length Rectangular Duct

4.1.1 ANC of ducted loudspeaker

Figure 13 shows the measured sound power reduction when the finite-length duct model (described in Sec. 2.1) is applied to the wooden duct pictured in Fig. 7. Predicted sound power reduction is shown for frequencies between 500 Hz and 2 kHz, while the measured sound power reduction is shown for frequencies between 1 and 1.7 kHz in 100 Hz increments. The measured reductions match the predicted theoretical maximum quite closely up to approximately 1.5 kHz. The lack of agreement above 1.5 kHz is likely due to the limited sampling frequency of the ANC controller (6 kHz). The upper frequency limit of the ANC algorithm is approximately $f_s/4$ (1.5 kHz) and one can expect deviations from ideal at frequencies above that cutoff[19].
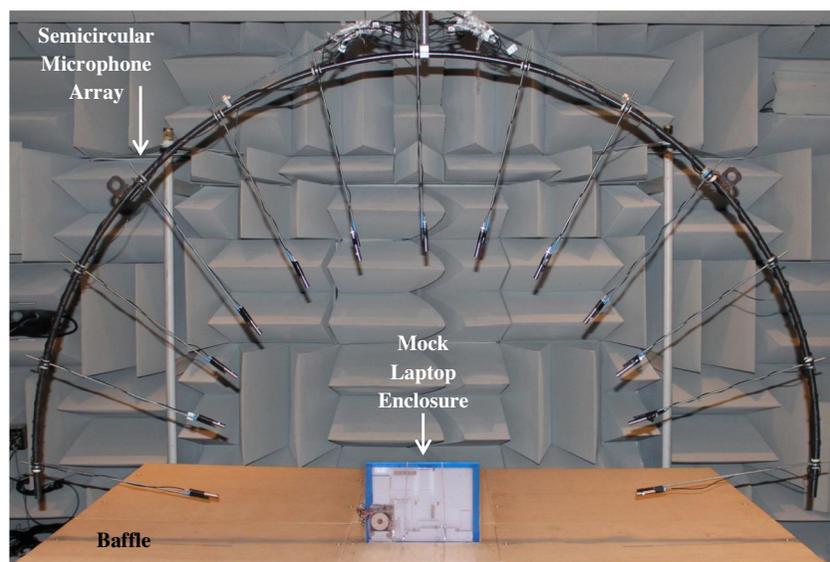

Fig. 12—*Photograph showing the experimental setup used to validate the two-dimensional modal model. The blower is placed in a mock laptop enclosure and mounted on a large wooden baffle (2.29 m × 2.29 m) such that the blower's exhaust vents below the baffle. A semicircular rotating array of microphones (56 cm radius) is suspended overhead.*
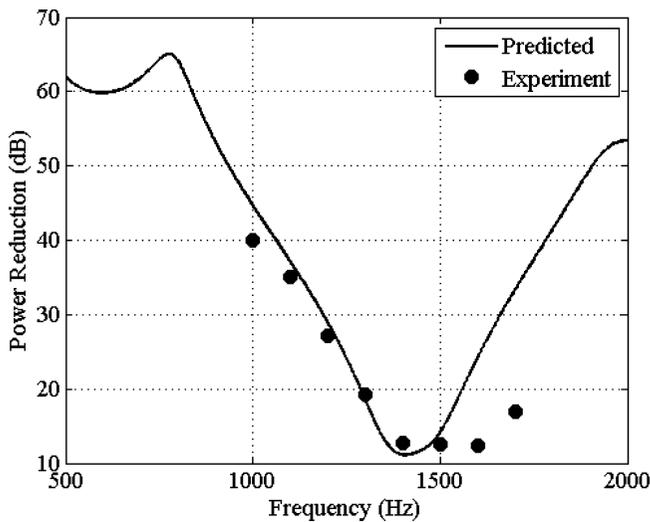
Fig. 13—Experimental results showing sound power reduction for the ideal duct pictured in Fig. 3. The line shows the theoretical prediction for power reduction, while the dots show experimental results at 100-Hz spacing between 1000 and 1700 Hz. The x-axis is in hertz while the y-axis is in decibels relative to the uncontrolled sound power.

4.1.2 ANC of ducted blower

Figure 14 shows the measured sound power reduction when the finite-length duct model (described in Sec. 2.1) is applied to the ducted centrifugal blower pictured in Fig. 9. The centrifugal blower emitted a bpf of approximately 1 kHz. The radius of the outer mesh corresponds to the sound pressure level of the uncontrolled sound field while the colored surface (radius and color) corresponds to the sound pressure level of the controlled sound field. The blower and duct assembly was oriented such that the primary source and the secondary source lie perpendicular to the x axis, as shown in Fig. 14. The sound power reduction is significant in magnitude (17 dB) and global in directionality, as the model predicts.

The decrease in sound power level reduction (from 40 to 17 dB when comparing Figs. 13 and 14) is likely due to differences in the primary source. The speaker tone used for Fig. 13 has a much higher signal-to-noise ratio than the centrifugal blower's bpf tone used for Fig. 14.

4.2 2-D Rectangular Enclosure

Figure 15(a) shows the measured sound power reduction when the 2-D rectangular enclosure model (described in Sec. 2.2) is applied to the enclosed centrifugal blower (pictured in Fig. 10) using the error sensor configuration shown in Fig. 4. The radius of the outer mesh corresponds to the sound pressure level of the uncontrolled sound field while the colored surface (radius and color) corresponds to the sound pressure level of the controlled sound field. When the blower emits a bpf of approximately 1 kHz, there is a 13 dB reduction in global sound power. Additionally, there is a 22 dB reduction in the sound pressure level in the direction of the operator position, i.e. the direction the operator would be when he/she uses the laptop. For these tests, it is located along the y-axis at a 50° angle from the baffle
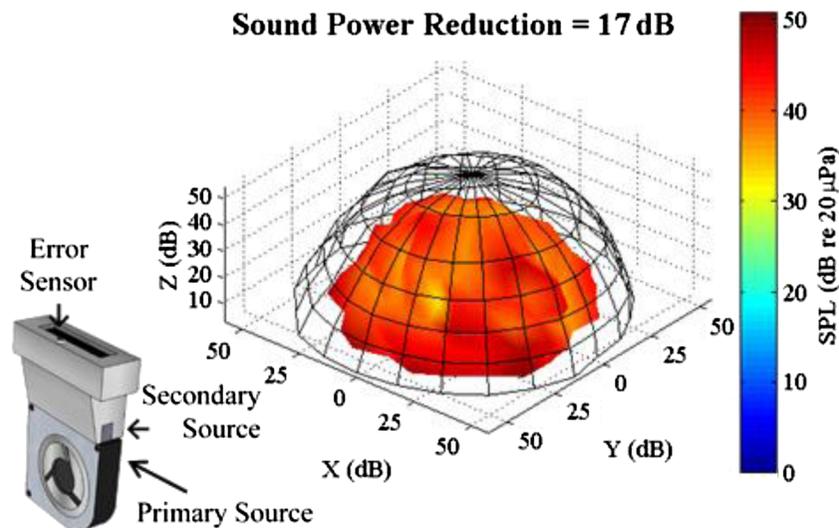

Fig. 14—Experimental result for control the blower exhaust pictured in Fig. 5. The radius of the outer mesh corresponds to the uncontrolled sound field while the colored surface (radius and color) corresponds to the controlled sound field. The axis units and color scale are in dB re 20 μPa. The blower and duct assembly is oriented as shown.
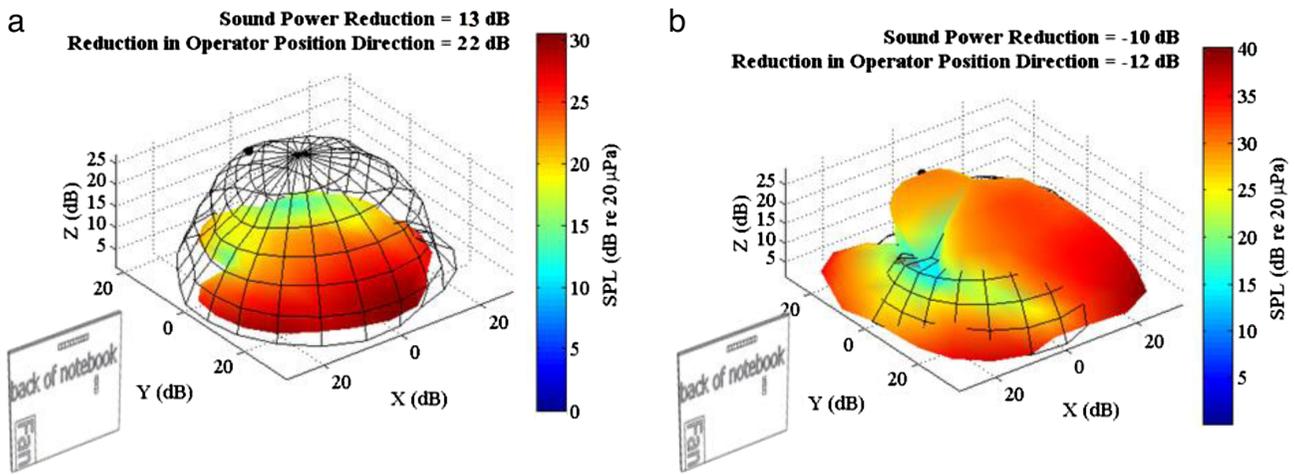
Fig. 15—Experimental result for control of blower's inlet when the model's recommendations [Fig. 15(a)] are followed as shown in Fig. 4 and are not followed as shown in Fig. 11 [Fig. 15(b)]. The outer mesh is the uncontrolled sound field while the colored surface is the controlled sound field. The operator position direction is indicated by the black dot on the back side of each figure. The axis units and color scale are in dB re 20 µPa. The laptop enclosure is oriented as shown.

plane. This location is indicated by a solid black dot in Fig. 15(a).

Figure 15(b) shows the measured sound power reduction of the enclosed centrifugal blower (pictured in Fig. 10) using the error sensor configuration shown in Fig. 11. This is contrary to the recommendations given by the 2-D rectangular enclosure model descried in Sec. 2.2. Note that the significant reduction obtained when the model's recommendations were followed [as seen in Fig. 15(a)] disappears. This confirms that the modeling approach outlined in this paper is useful in determining the proper configuration of the control system in order to achieve significant attenuation of the sound field.

5 CONCLUSIONS

Theoretical models have been presented for active noise control of a point source in a finite-length rectangular duct and in a two-dimensional rectangular enclosure with lossy sides. These models have been applied to a centrifugal blower mounted in two different configurations: a blower mounted in a small, rectangular duct (where noise from the blower's exhaust was controlled) and a blower mounted in a mock laptop enclosure (where noise from the blower's inlets was controlled).

Experiments validated the finite-length duct model when a loudspeaker was used as the primary source, with sound power reductions between approximately 12 and 40 dB, depending on frequency. Deviations above 1.5 kHz can be attributed to the limited sampling frequency of the ANC controller. Experiments also produced 17 dB of sound power reduction when the finite-length duct model

was applied to the bpf radiated from the exhaust of the ducted centrifugal blower. Differences in sound power reduction between control of the loudspeaker and control of the blower can be attributed to differences in the SNR of the loudspeaker and the blower.

Experiments also validated the 2-D rectangular enclosure model. When its recommendations were followed, the radiated sound power from the inlets of the centrifugal blower in the mock laptop enclosure was reduced by 13 dB. The blower's radiated sound pressure level at the operator position was also reduced by 22 dB. However, when the model's recommendations were not followed, the sound power radiated from the blower's inlets was boosted by 10 dB while its radiated sound pressure level at the operator position was boosted by 12 dB.

6 REFERENCES

1. G.W. Evans and D. Johnson, "Stress and open-office noise", *J. Appl. Psych.*, **85**(5), 779–783, (2000).
2. G.C. Maling Jr., "Historical developments in the control of noise generated by small air-moving devices", *Noise Control. Engr. J.*, **42**(5), 159–169, (1994).
3. K.L. Gee and S D. Sommerfeldt, "Application of theoretical modeling to multichannel active control of cooling fan noise", *J. Acoust. Soc. Am.*, **115**, 228–236, (2004).
4. K.L. Gee and S.D. Sommerfeldt, "A compact active control implementation for axial cooling fan noise", *Noise Control Engr. J.*, **51**(6), 325–334, (2003).
5. B.M. Shafer, K.L. Gee and S.D. Sommerfeldt, "Verification of a near-field error sensor placement method in active control of compact noise sources", *J. Acoust. Soc. Am.*, **127**(2), EL66–EL72, (2010).
6. G.H. Koopmann, D.J. Fox and W. Nezse, "Active source cancellation of the blade tone fundamental and harmonics in centrifugal fans", *J. Sound Vibr.*, **126**(2), 209–220, (1988).

7. G.H. Koopmann, W. Neise and W. Chen, "Active noise control to reduce the blade tone noise of centrifugal fans", *J. Vib. Acoust. Stress Rel. Des.*, **110**(7), 377–383, (1988).

8. J. Wu, "Application of feedforward adaptive active-noise control for reducing blade passing noise in centrifugal fans", *J. Sound Vibr.*, **239**(5), 1051–1062, (2001).

9. D. Wolfram and T.H. Carolus, "Experimental and numerical investigation of the unsteady flow field and tone generation in an isolated centrifugal fan impeller", *J. Sound Vibr.*, **329**(21), 4380–4397, (2010).

10. H.A. Cordourier-Maruri and F. Orduna-Bustamente, "Active control of periodic fan noise in laptops: Spectral width requirements in a delayed buffer implementation", *J. Appl. Res. Tech.*, **7**(2), 124–135, (2009).

11. P. Morse and K. Ingard, *Theoretical Acoustics*, MacMillan, London, (1986), p. 500.

12. J.J. Esplin, J.K. Boyle, S.D. Sommerfeldt and K.L. Gee, "Active control of centrifugal fan noise: Modeling design guidelines", *Proc. Mtgs. Acoust.*, **12**, 040009, (2011).

13. S. Wang, J. Tao and X. Qiu, "Performance of a planar virtual sound barrier at the baffled opening of a rectangular cavity", *J. Acoust. Soc. Am.*, **138**(5), 2836–2847, (2015).

14. J.A. Kemp, D.M. Campbell and N. Amir, "Multimodal radiation impedance of a rectangular duct terminated in an infinite baffle", *Acta Acustica*, **87**, 11–15 (2001).

15. A.D. Pierce, *Acoustics: An Introduction to its Physical Principles and Applications*, Acoustical Society of America, Melville, New York, (1989).

16. P.A. Nelson and S.J. Elliott, *Active Control of Sound*, Academic Press Limited, London, (1992).

17. S.D. Sommerfeldt and K.L. Gee, "Active control of axial and centrifugal fan noise", *Proc. Mtgs. Acoust.*, **19**, 030009, (2013).

18. T.W. Leishman, S. Rollins and H.M. Smith, "An experimental evaluation of regular polyhedron loudspeakers as omnidirectional sources of sound", *J. Acoust. Soc. Am.*, **120**(3), 1411–1422, (2006).

19. C.H. Hansen, "Control system implementation", *Active Control of Noise and Vibration*, 2nd ed., CRC Press, Boca Raton, Florida, (2013), Chapter 13.